Supporting Information

Nanostructure-Enabled Apparent Slip through Dynamic Hydration Reorganization

Youngho Han[1,2,†], Aoife Lundberg[3,†], Jong Sik Kim[2], Paul Cannon[4], Doojin Lee[*2,1], Enda McGlynn[†3], and Nikhil Bhalla[‡1]

[1]Nanotechnology and Integrated Bioengineering Centre (NIBEC), School of Engineering, Ulster University, 2–24 York Street, Belfast BT15 1AP, Northern Ireland, UK
[2]Department of Polymer Science and Engineering, Chonnam National University, Gwangju 61186, South Korea
[3]School of Physical Sciences, Dublin City University, Glasnevin, Dublin 9, Ireland
[4]Advanced Research Center for Nanolithography (ARCNL), Science Park 106, 1098 XG Amsterdam, The Netherlands
[†]Y.H. and A.L. contributed equally to this paper.

Downloaded from pubs.acs.org/aamick/article-supplement/5456588/pdf/am-2026-16664d_si_001/ by DUBLIN CITY UNIV user on 05 November 2026

[*]Corresponding author: dlee@chonnam.ac.kr
[†]Corresponding author: enda.mcglynn@dcu.ie
[‡]Corresponding author: n.bhalla@ulster.ac.uk

Contents

1 Morphology of the SiO_2 dendrites on the surface 3

2 Concentration dependent acoustic response by flow rates 3

3 Dissipation–frequency trajectories resolved by electrolyte concentration 4

4 Real-time acoustic response during BSA adsorption 6

5 Estimated composition and ionic strength of the PBS test solutions 6

6 QCM-D response of the bare gold-coated crystal 6

7 Surface composition of the SiO_2-coated surface 8

8 DFT adsorption energies of water on silica surface groups 9

9 References 11

Downloaded from pubs.acs.org/aamick/article-supplement/5456588/pdf/am-2026-16664d_si_001/ by DUBLIN CITY UNIV user on 05 November 2026

1 Morphology of the SiO_2 dendrites on the surface

Figure S1 shows top-view and side-view SEM images of the SiO_2 crystal surface. The top-view images confirm that the dendrite coating covers the surface uniformly (Figure S1a) and reveal that each dendrite consists of nanoparticles and that the dendrites exhibit diverse morphologies (Figure S1b). Furthermore, side-view images provide additional information on the structure and vertical extent of the dendrites (Figure S1c,d).

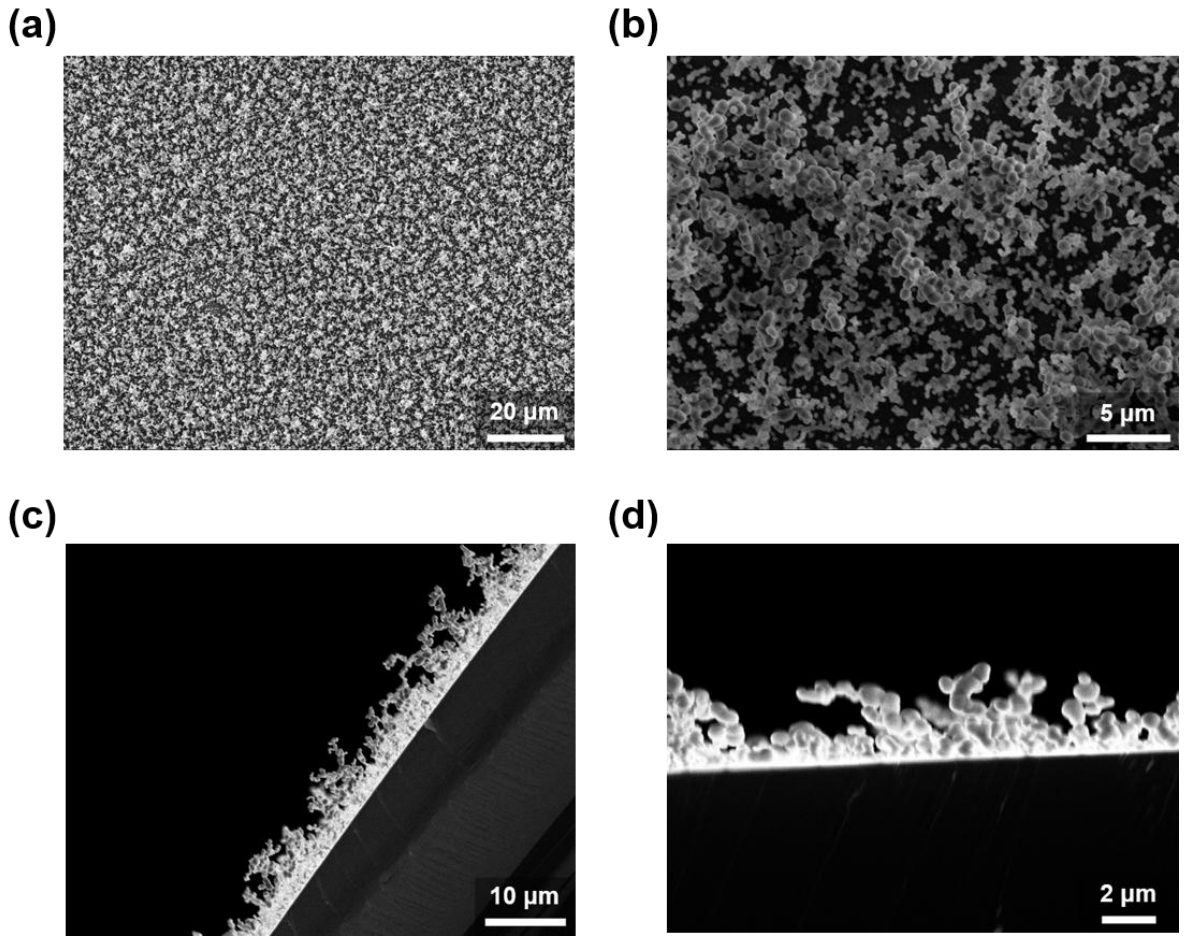


Figure S1: Surface morphology of the SiO_2 dendrites-coated crystal. (a,b) top-view SEM images at low and high magnification (c,d) side-view SEM images at low and high magnification.

2 Concentration dependent acoustic response by flow rates

Figure S2 presents the same overtone data of Figure.3 in the main text, replotted with electrolyte concentration on the x-axis and flow rate as the variable. This representation is complementary rather than additional. Figure.3 considers the concentration at fixed flow rates, whereas Figure S2 shows hydrodynamic forcing at fixed concentration. Viewing the same measurements along both axes is necessary because the main-text analysis attributes the acoustic response to a two-parameter mechanism in which ionic strength defines the molecular state of the hydration interface and flow determines the reorganizing of hydration structures.

The entire data of Figure S2 show a clear and discontinuous discontinuity between the low-intermediate flow rate (1–16 mL/h) group and the highest flow rate (32 mL/h). This observation supports the flow-activated transition characteristic that occurs above a certain critical flow force, rather than a modest change with increasing flow [1]. In the overtone difference, as the overtone increases, the absolute variation increases, but the value of n5 decreases in clarity. This phenomenon is because the larger the overtone, the greater the possibility of noise being involved. Dissipation shift decreases or remains, inversely

Downloaded from pubs.acs.org/aamick/article-supplement/5456588/pdf/am-2026-16664d_si_001/ by DUBLIN CITY UNIV user on 05 November 2026

proportional to frequency shift. At 32 mL/h, the dissipation level is the lowest.

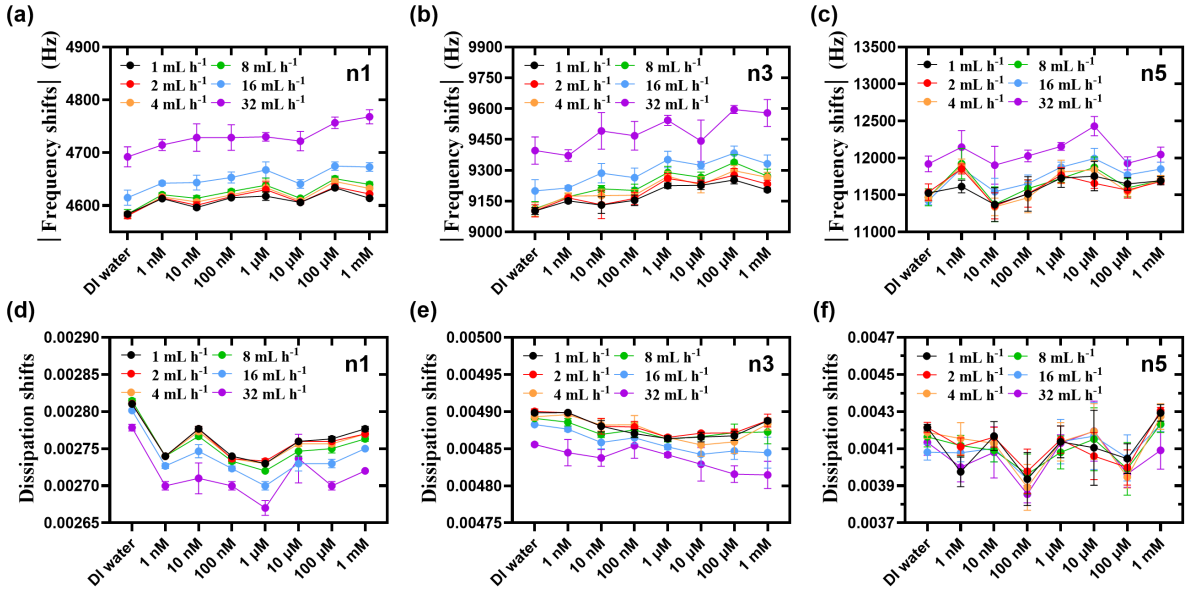


Figure S2: Shifts in frequency and dissipation at fixed electrolyte concentrations as a function of flow rate. (a–c) Frequency shifts (Δf) at overtones (a) $n = 1$, (b) $n = 3$, and (c) $n = 5$.(d–f) Dissipation shifts (ΔD) at overtones (d) $n = 1$, (e) $n = 3$, and (c) $n = 5$.

3 Dissipation–frequency trajectories resolved by electrolyte concentration

Figures S3–S5 present the original data used to obtain the slope, $d(\Delta D)/d(|\Delta f|)$, for each concentration in Figure 4(a–c) of the main text. The black, blue, and red symbols mean the result of independent experiments. Without prior averaging, the frequency and dissipation changes across all measured flow rates (1, 2, 4, 8, 16, and 32 mL/h) are plotted directly. If the results of independent experiments are averaged, the flow-dependent changes in $\Delta D/|\Delta f|$ could be hidden. Therefore, the dataset is presented through linear regression fitting for each trial, and the fitted slopes form the basis of the summarized data in the main text.

Figure S3 shows a clear negative slope under all concentration conditions. In addition, the data measured at each concentration have linearity, and the independent data are almost matched. This confirms that the data are highly reproducible at overtone 1, and these results are a reaction to a unique interface. Even in Figure S4, the slope remains negative for most concentrations, but the dispersion of the data increases. Nevertheless, the slope remains consistently negative for overtone 3. Figure S5 shows a completely different pattern than the previous two overtones. It greatly increases the scatter of the data, and the fitted slope becomes close to zero or positive. Higher-order overtones exhibit pronounced sensitivity to minute local flux variations and surface noise. The slope is extremely small, so even a minor variation can cause its sign to change.[2] What matters is not the sign change, but the tendency of the slope to change with the overtones. The higher the overtones, the closer the slope tends to be to zero in negative numbers.

Downloaded from pubs.acs.org/aamick/article-supplement/5456588/pdf/am-2026-16664d_si_001/ by DUBLIN CITY UNIV user on 05 November 2026

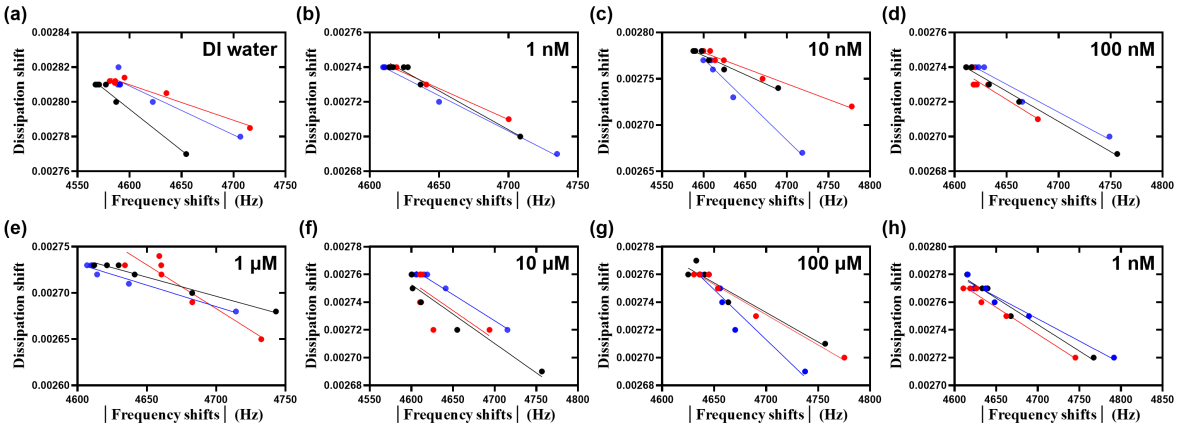


Figure S3: Dissipation–frequency trajectories at $n = 1$ across varying electrolyte concentrations and flow rates. Energy dissipation shift (ΔD) plotted against absolute frequency shift ($|\Delta f|$) at (a) DI water, (b) 1 nM, (c) 10 nM, (d) 100 nM, (e) 1 μM, (f) 10 μM, (g) 100 μM, and (h) 1 mM PBS

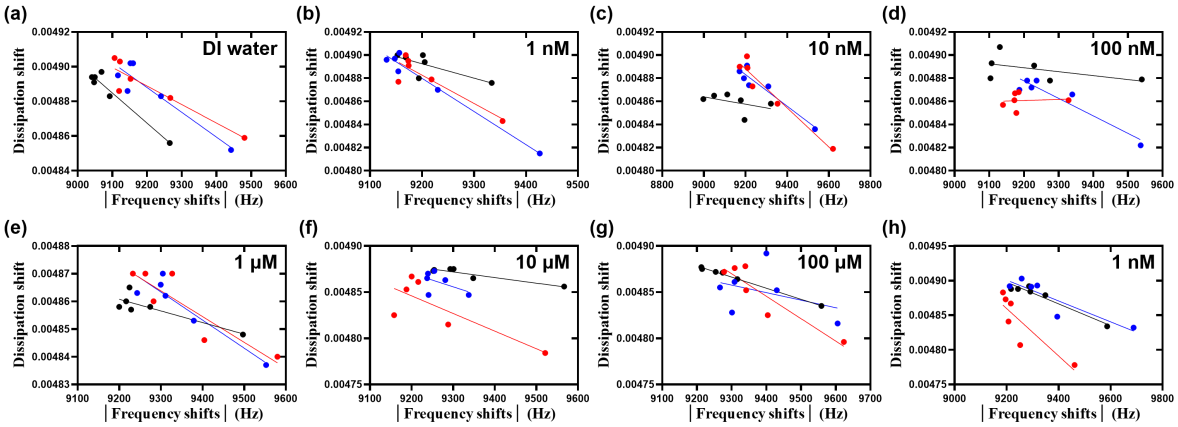


Figure S4: Dissipation–frequency trajectories at $n = 3$ across varying electrolyte concentrations and flow rates. Energy dissipation shift (ΔD) plotted against absolute frequency shift ($|\Delta f|$) at (a) DI water, (b) 1 nM, (c) 10 nM, (d) 100 nM, (e) 1 μM, (f) 10 μM, (g) 100 μM, and (h) 1 mM PBS

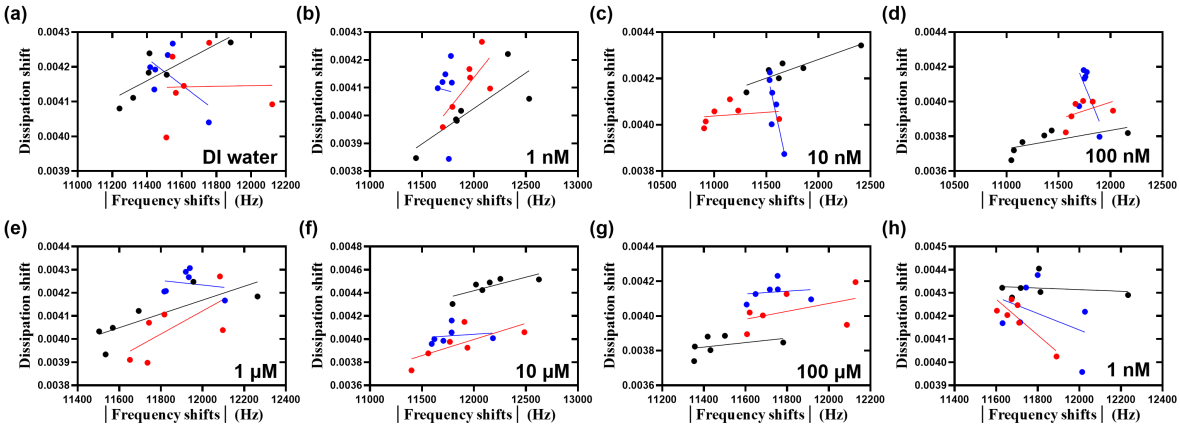


Figure S5: Dissipation–frequency trajectories at $n = 5$ across varying electrolyte concentrations and flow rates. Energy dissipation shift (ΔD) plotted against absolute frequency shift ($|\Delta f|$) at (a) DI water, (b) 1 nM, (c) 10 nM, (d) 100 nM, (e) 1 μM, (f) 10 μM, (g) 100 μM, and (h) 1 mM PBS

Downloaded from pubs.acs.org/aamick/article-supplement/545688/pdf/am-2026-16664d_si_001/ by DUBLIN CITY UNIV user on 05 November 2026

4 Real-time acoustic response during BSA adsorption

Figure S6 shows the amount of change in frequency and dissipation generated during the adsorption of BSA protein on the surfaces of bare crystal and SiO_2-coated crystal as data over time. Following the onset of adsorption, both samples reach a stable plateau that is held continuously for over 300 s. The response traces recorded across different flow rates nearly overlap, demonstrating that hydrodynamic flow forces do not induce progressive protein desorption. This indicates that the protein-adsorbed interface forms mechanically stable and maintains its own state even under high flow rates. These results originate from the reconstruction of the hydration layer[3], ultimately demonstrating that a larger acoustic load does not necessarily imply a more rigidly fixed hydrodynamic boundary[4].

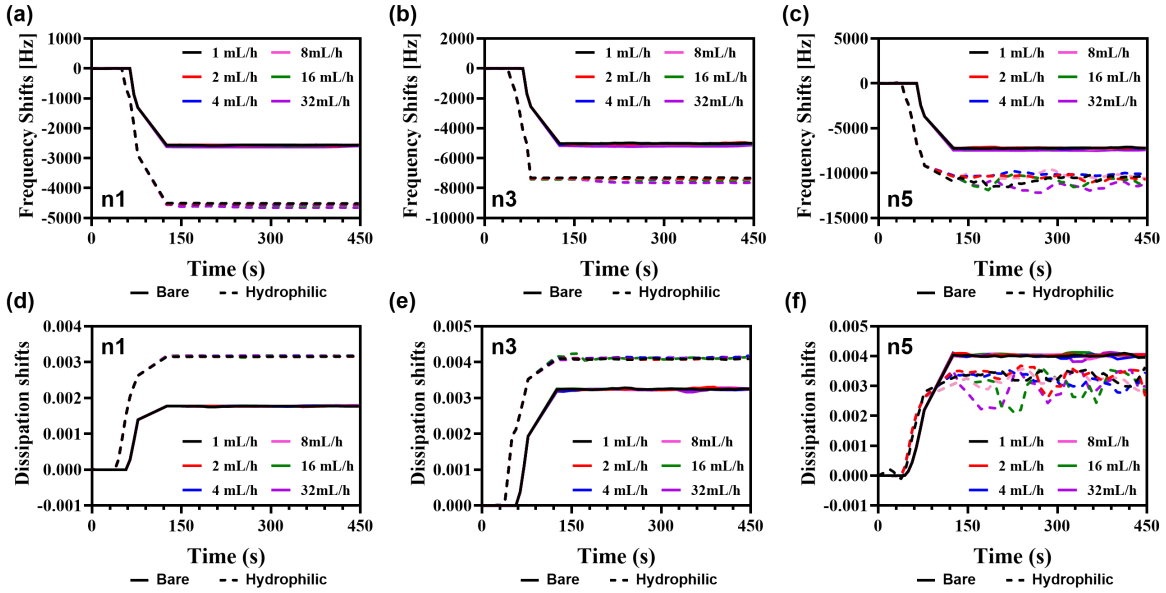


Figure S6: Real-time QCM-D response during BSA adsorption on bare (solid lines) and SiO_2-coated (dashed lines) sensors across flow rates from 1, 2, 4, 8, 16, and 32 mL/h. (a–c) Frequency shifts (Δf) at overtones (a) $n = 1$, (b) $n = 3$, and (c) $n = 5$. (d–f) Dissipation shifts (ΔD) at overtones (d) $n = 1$, (e) $n = 3$, and (f) $n = 5$

5 Estimated composition and ionic strength of the PBS test solutions

Table S1 shows estimated composition and ionic strength. These values were calculated as

$$I = \frac{1}{2} \sum_i c_i z_i^2 \tag{S1}$$

where c_i is the molar concentration and z_i is the charge number of ion i. The ionic strength of stock solution is estimated to be approximately 160 mM, and it decreases tenfold with each dilution step.

6 QCM-D response of the bare gold-coated crystal

To determine whether the electrolyte and flow-dependent responses of the dendritic SiO_2 interface originate from general acoustic or flow-cell effects, control measurements were performed using bare gold-coated quartz crystals. Measurements were conducted in DI water and PBS solutions (1 nM–1 mM) under the same conditions used for the SiO_2-coated crystals.Under static conditions (Figure S7), the frequency shifts on the bare gold-coated surface were approximately 2.5, 5, and 7.1 kHz at n1, n3, and n5, respectively. These values were smaller than those on the SiO_2-coated surface.

Downloaded from pubs.acs.org/aamick/article-supplement/5456588/pdf/am-2026-16664d_si_001/ by DUBLIN CITY UNIV user on 05 November 2026

Table S1: Estimated composition and ionic strength of the PBS test solutions, calculated from the composition of the 10 mM PBS stock solution and the tenfold serial dilution factor.

Sample	Phosphate (mM)	KCl (mM)	NaCl (mM)	Ionic strength (mM)
1 mM	1.0	2.7×10^{-1}	13.7	16
100 μM	1.0×10^{-1}	2.7×10^{-2}	1.37	1.6
10 μM	1.0×10^{-2}	2.7×10^{-3}	1.37×10^{-1}	1.6×10^{-1}
1 μM	1.0×10^{-3}	2.7×10^{-4}	1.37×10^{-2}	1.6×10^{-2}
100 nM	1.0×10^{-4}	2.7×10^{-5}	1.37×10^{-3}	1.6×10^{-3}
10 nM	1.0×10^{-5}	2.7×10^{-6}	1.37×10^{-4}	1.6×10^{-4}
1 nM	1.0×10^{-6}	2.7×10^{-7}	1.37×10^{-5}	1.6×10^{-5}

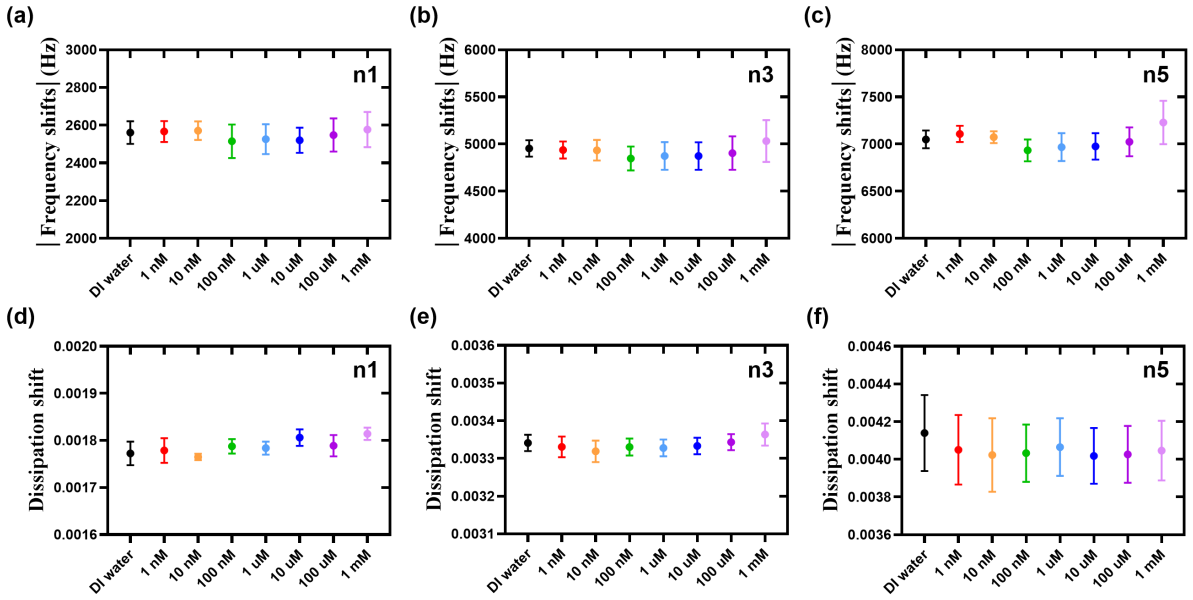


Figure S7: QCM-D response of the bare gold-coated crystal under static conditions in DI water and PBS solutions ranging from 1 nM to 1 mM. (a–c) Frequency shifts at n1, n3, and n5 (d–f) Dissipation shifts at n1, n3, and n5

Under flow (Figure S8), $|\Delta f|$ on the bare surface increased slightly with flow rate, suggesting a contribution from general flow-cell effects, such as the force exerted by the injected flow on the crystal. However, the increase was smaller than that observed on the dendritic SiO_2 surface, particularly at $n = 5$. In contrast, ΔD on the bare surface remained nearly constant across the flow range, while it decreased or remained nearly unchanged on the dendritic SiO_2 surface. These results suggest that the concentration-dependent response at higher overtones and the increased frequency loading without a corresponding increase in dissipation under flow are mainly associated with the dendritic SiO_2 interface rather than general acoustic or flow-cell effects.

Downloaded from pubs.acs.org/aamick/article-supplement/5456588/pdf/am-2026-16664d_si_001/ by DUBLIN CITY UNIV user on 05 November 2026

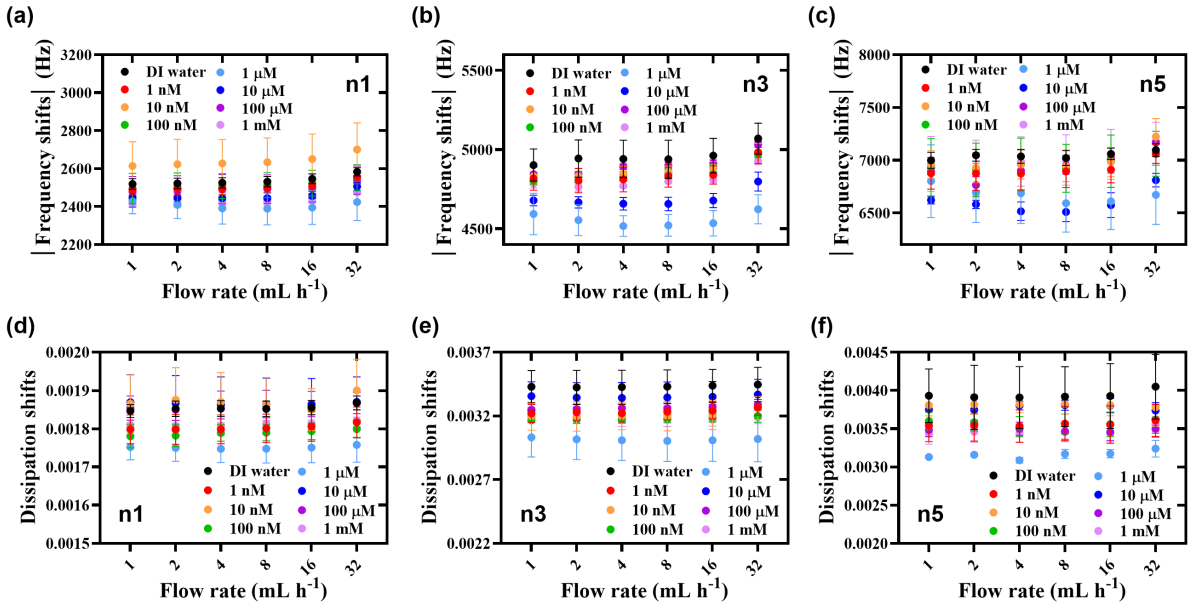


Figure S8: Flow-dependent QCM-D response of the bare gold-coated crystal in DI water and PBS solutions ranging from 1 nM to 1 mM (a–c) Frequency shifts at n1, n3, and n5 (d–f) Dissipation shifts at n1, n3, and n5

7 Surface composition of the SiO_2-coated surface

The SiO_2-coated surface was analyzed by XPS before and after UV treatment to assess atomic concentration on the surface (Figure S9). The surface mainly consisted of Si and O, with a carbon content below 6 at% before UV treatment and approximately 2 at% after treatment. The C 1s spectra show a peak at approximately 284 eV, characteristic of carbon, which decreased after UV treatment (Figure S9 b and c). The Si 2p spectra show a single peak at approximately 103 eV, corresponding to SiO_2 (Figure S9 d and e). Notably, the O/Si atomic ratio was approximately 2.5 before and 2.7 after UV treatment, exceeding the stoichiometric value of 2 for SiO_2. Since this excess oxygen cannot be accounted for by the small carbon content, which decreased after UV treatment while the O/Si ratio increased, it is attributed to surface hydroxyl groups, supporting the presence of a hydroxylated silica surface.

Downloaded from pubs.acs.org/aamick/article-supplement/5456588/pdf/am-2026-16664d_si_001/ by DUBLIN CITY UNIV user on 05 November 2026

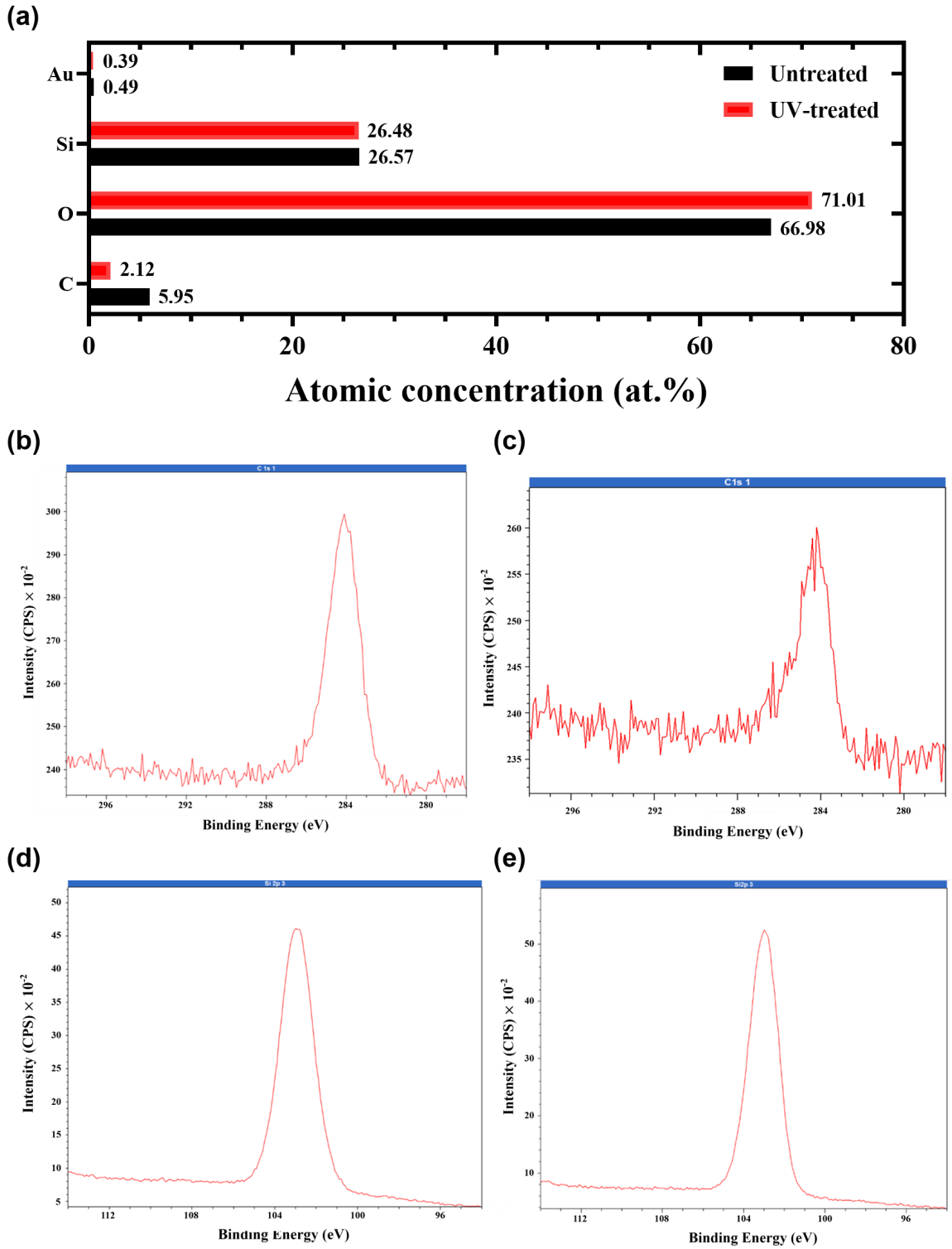


Figure S9: XPS analysis of the SiO_2 dendrite-coated quartz crystal before and after UV/ozone treatment for 1 h. (a) Surface elemental composition before (black) and after (red) UV treatment. (b,c) C 1s spectra (b) before and (c) after UV treatment. (d,e) Si 2p spectra (d) before and (e) after UV treatment.

8 DFT adsorption energies of water on silica surface groups

The purpose of the DFT calculations was not to reproduce the macroscopic wettability, but to compare the intrinsic affinity of water toward the local chemical groups constituting the surface, silanol (Si–OH) and siloxane (Si–O–Si) groups. The calculations show that water adsorbs more strongly on Si–OH (Model

Downloaded from pubs.acs.org/aamick/article-supplement/545688/pdf/am-2026-16664d_si_001/ by DUBLIN CITY UNIV user on 05 November 2026

1,E$_{ads}$ ≈ -26 kJ/mol) than on Si–O–Si (Model 2 and 3, ≈ -15.7 and ≈ -14.6 kJ/mol), corresponding to approximately 0.6 of the Si—OH value (Model 1). This relative trend was used only qualitatively to support the analysis.

Table S2: Calculated adsorption energies of water on silica cluster models.

Model	Surface group (water approach)	E_{ads} (kJ mol^{-1})	E_{ads} (eV)	Normalized
1	Si–OH (Model1)	-26.0	-0.270	1.00
2	Si–O–Si (Model2)	-15.7	-0.163	0.60
3	Si–O–Si (Model3)	-14.6	-0.151	0.56

Downloaded from pubs.acs.org/aamick/article-supplement/545588/pdf/am-2026-16664d_si_001/ by DUBLIN CITY UNIV user on 05 November 2026

9 References

[1] Tirtaatmadja, V.; Tam, K.; Jenkins, R. Superposition of oscillations on steady shear flow as a technique for investigating the structure of associative polymers. *Macromolecules* **1997**, *30*, 1426–1433.

[2] Johannsmann, D.; Reviakine, I.; Rojas, E.; Gallego, M. Effect of Sample Heterogeneity on the Interpretation of QCM-D Data: Comparison of Combined Quartz Crystal Microbalance/Atomic Force Microscopy Measurements with Finite Element Method Modeling. *Analytical Chemistry* **2008**, *80*, 8891–8899.

[3] Nagasawa, D.; Azuma, T.; Noguchi, H.; Uosaki, K.; Takai, M. Role of Interfacial Water in Protein Adsorption onto Polymer Brushes as Studied by SFG Spectroscopy and QCM. *The Journal of Physical Chemistry C* **2015**, *119*, 17193–17201.

[4] Adamczyk, Z.; Sadowska, M.; Żeliszewska, P. Applicability of QCM-D for Quantitative Measurements of Nano- and Microparticle Deposition Kinetics: Theoretical Modeling and Experiments. *Analytical Chemistry* **2020**, *92*, 15087–15095.

Downloaded from pubs.acs.org/aamick/article-supplement/545588/pdf/am-2026-16664d_si_001/ by DUBLIN CITY UNIV user on 05 November 2026